The physical characterisation of a microscale parallel bioreactor platform with an industrial CHO cell line expressing an IgG4

The physical characterisation of a microscale parallel bioreactor platform with an industrial CHO cell line expressing an IgG4.

Alvin W. Nienow[1,2], Christopher D. Rielly[1], Kathryn Brosnan[1], Kenneth Lee[1], Neil Bargh[3], Karen Coopman[1] and Christopher J. Hewitt[1*]

[1]*Centre for Biological Engineering, Department of Chemical Engineering, Loughborough University, Leicestershire, LE11 3TU, UK*

[2]*Centre for Bioprocess Engineering, Department of Chemical Engineering, University of Birmingham, B15 2TT, UK*

[3]*TAP Biosystems, York Way, Royston, Hertfordshire SG8 5WY, UK*

**Author for correspondence. Phone: +44-121-440-2344;E-mail: A.W.Nienow@bham.ac.uk)*

Abstract

There is a growing body of evidence that the ambr™ workstation from TAP Biosystems performs well in terms of helping to select appropriate clones for scale-up studies. In line with these other studies, we found that the fed-batch culture of CHO cells in a 15 mL ambr bioreactor gave similar cell growth and productivity to that achieved in a 5 L stirred bioreactor whilst the results from shake flasks were significantly different. However, here for the first time, we have also investigated the physical characteristics of this microscale bioreactor system and found some important differences compared to those of larger scale stirred bioreactors. For example, the flow regime in the ambr vessel is transitional rather than turbulent and the sparged air/oxygen superficial gas velocity is relatively very low; and for the fed-batch culture giving results similar to the 5L bioreactor, the specific power input was much higher (~ 400 W/m^3) when compared to that used at commercial scale (typically ~ 50 W/m^3). These conditions give a k_La value which along with an enhanced oxygen driving force are able to meet the oxygen demand of the cells and give control of dO_2. The flexibility of the ambr dO_2 control system also allows other settings to be chosen. Given the differences in physical characteristics between the ambr and larger stirred bioreactors, we suggest that this similarity in biological performance is due to their similar control capabilities and the 'equivalence of the stress parameters' across the scales when compared with shake flasks.

Keywords: ambr microscale bioreactor, CHO cell culture, transitional flow, CFD, specific power input, mass transfer.

Highlights

- Confirms that unlike shake flasks, ambr™ growth and productivity mimics a 5L stirred bioreactor
- Physical characteristics in an ambr™ and a 5L stirred bioreactor are very different
- Transitional rather than turbulent flow with higher specific power inputs (up to ~ 400 W/m^3)
- Surface mass transfer contributes much more to the overall rate of oxygen transfer
- The high specific power input does not lead to a deterioration in performance

1. Introduction

Over the last 15 years or so a new global healthcare industry worth approximately £30 billion a year has emerged, based on the production of human proteins in genetically engineered cells [1]. Products include therapeutic antibodies which are generated in modified CHO-cell lines and which can now be successfully cultured at scales of up to 25,000 litres [2]. Key to the current and continuing success of the industry has been the initial screening of protein-expressing clones to select for high producers and the optimisation of fermentation conditions, including medium composition, feeding strategies, and temperature, pH and dO_2 profiles to generate high yields of biomass and product.

Initial screening and process development is often carried out in shaken systems [3, 4] as it allows many experiments to be run in parallel and encourages the use of complex experimental protocols, such as factorial designs and surface response methodology. Although over 90% of all experimental trials taking place in 50 mL shake flasks [5], the industry standard for large-scale fermentations is the stirred tank bioreactor and changes in bioperformance often occur when mechanical agitation and aeration are introduced into a bioreactor as compared to the non-agitated and non-sparged conditions in a shake flask [6]. Indeed during initial screening programmes designed to rapidly identify high protein-expressing clones, candidate over-producing cell lines are often discarded when their performance in larger scale mechanically agitated systems does not match that predicted from the shake flask. In the past such a detrimental change was often attributed to so called ‘shear damage’ although much work has now shown that animal cells are more likely to be damaged by the action of bursting bubbles at the liquid free surface than by the action of fluid shear rates or stresses generated by impellers [7]. Importantly, it should also be noted that damage by bursting bubbles is now routinely eliminated by the addition of antifoaming

agents such as Pluronic F68 to the culture medium [2].

Clearly there are significant physical differences between shaken and mechanically agitated bioreactor platforms, so it is perhaps unsurprising that the resultant biological performance may be very different. These physical differences include the mixing strategy (shaken vs. stirred), gassing strategy (surface aeration vs. sparging) and very often, the ability to routinely control quantities such as pH or dO_2 through online monitoring and automated additions of controlling agents (historically largely absent vs. present). Though fully instrumented shake flask systems, designed to measure and potentially control pH and dO_2 levels online have become available [8, 9], they are relatively complicated to operate and have not become routinely used by industry. Certainly, there are particular physical aspects such as the impact of fluid dynamic stresses from agitation and sparging as well as estimates of k_La that will be found in large scale stirred bioreactors which can only be effectively obtained in stirred bench scale bioreactors of a few litres and larger, hence, a critical aspect of upstream process development is still done in 1 - 30 L stirred tank bioreactors [10].

There has recently been a trend for the development of microscale bioreactor systems which are mechanically and functionally similar to large scale bioreactors [3, 4, 11]. Ideally these should maintain, the key characteristics of a larger bioreactor such as mechanical agitation, sparged gas entry into the impeller region and allow for the monitoring and control of dO_2, pH and pCO_2. Automated operation also increases the ease of handling, reduces human error and enables parallel small scale fermentations to be carried out, reducing developmental costs and time to pilot scale if they give similar performance to that achieved at the larger scale. A small number of microscale bioreactor systems are now commercially available of which Micro-24^{TM} (Pall Life Sciences, UK) and the BioLector ^{TM} (m2p-Labs GmbH, Germany) are shaken systems and the ambr (TAP Biosystems, UK) is mechanically agitated with sparged

aeration. The SimCell^{TM} (Seahorse Bioscience, USA) was similar to the ambr but is no longer being produced. These have all recently been extensively reviewed elsewhere [3] but notably only the ambr system uses an impeller and offers fully automated control of pH and dO_2 with the possibility of fed-batch operation; it is the subject of study here.

Although these small scale bioreactors potentially overcome some of the issues compared to using shake flasks in clone screening, it is important that the physical characteristics of such a system are understood as these vary with scale. Factors such as specific energy dissipation rate, mass transfer and blending characteristics are often difficult to determine quantitatively at small scale. Hence we have used a combination of experimental and computational methods to characterise the most important physical variables (power number, k_La and mixing time) on an individual ambr bioreactor vessel. We have also compared biologically an ambr-24 platform with its shake flask and stirred tank bioreactor counterparts using a common antibody expressing CHO-cell line. Differences in biological performance and physical characteristics are discussed in terms of each culture system. During the experimental study of the physical characteristics of the ambr, in order to develop more robust relationships, the conditions utilised are sometimes outside of the normal operating ranges and that is indicated as appropriate in the text.

2. Materials and Methods

2.1. Cultivation of CHO cells

An IgG4-expressing CHO-cell line, LB01, was provided by Lonza Biologics (Slough, UK). In all cases cells were cultured in CD-CHO medium (Invitrogen, Life Technologies, USA) supplemented with 25µM MSX (Sigma-Aldrich, Poole, UK) which was allowed to equilibrate at culture conditions for 24 hours before inoculation with cells at a density of 5 ×

10^5 cells/mL. Cells were either cultured using an ambr Workstation24^{TM} (TAP Biosystems, Royston, UK) (Fig. 1a), a 5 L Sartorius Stedim BioStat C stirred, double-jacketed, dish bottomed glass bioreactor (Sartorius, Germany) without baffles, or in Corning 250 ml shake flasks using an orbital shaker (Stuart, Bibby Scientific Limited, Stone, UK). The working volume of each was 15 ml, 3L and 70 ml respectively and the temperature was controlled at 37^{o}C. All cultures were fed with 10% CHO-CD Efficientfeed^{TM} B (Invitrogen, Life Technologies, USA) on day 0 and 10% concentrated CD Efficientfeed^{TM} C (Invitrogen, Life Technologies, USA) on days 3, 6 and 9 of culture. Antifoam C (1% solution, Sigma-Aldrich, Poole, UK) was added on demand to prevent foaming.

For the ambr and stirred bioreactor cultures, the pH was controlled at 6.9 using a combination of sparged CO_2 and liquid sodium bicarbonate (1M) addition on demand. Dissolved oxygen was controlled at 50% saturation using a fixed impeller speed (1200 rpm for the ambr and 250 rpm for the bioreactor, which thereby matched the tip speeds at ~ 0.7 m/s (a traditional scale-up rule [12], here used to scale down) and nitrogen flow rate (0.15 mL/min for the ambr and 30 mL/min for the bioreactor)) supplemented with varying oxygen flow rates as required. The ambr impeller was positioned in the vessel as shown in Fig. 1a at ~5 mm from the bottom of the vessel with two blades set at 45° to the vertical pumping upwards with a swept diameter, D = 11.4 mm (Fig. 1b). The Sartorius bioreactor had a three-blade up-pumping marine impeller with a swept diameter, D = 55 mm and at a clearance of ~55 mm from the bottom of the vessel. Online monitoring of the culture in the ambr vessel was achieved with disposable optical probes to measure pH and dissolved oxygen (dO_2) (PreSens GmbH, Germany), with measurements taken at 90 s intervals. Additionally, during biological experiments, the whole ambr system was located inside a class II biological safety cabinet to prevent contamination of the cultures during feeding and

sampling. In the Sartorius bioreactor, a polargraphic dissolved oxygen probe (Hamilton, Switzerland) and pH probe (Hamilton, Switzerland) were used. Shake flasks were agitated at 85 rpm within a static incubator controlled at 37°C with a 5% CO_2/air mixture and relative humidity of 95%.

2.2. Sample analysis

In all cases samples were taken daily for cell counts. Additional samples were taken every 2 days for pH measurement and protein titre (as of day 6) with cultures typically terminated on day 18. Cell counts were by a ViCell XR Automated Cell Viability Analyser (Beckman Coulter, High Wycombe, UK) using trypan blue exclusion to determine viable and total cell number.

Protein quantification was from cell free extracts by Protein A HPLC. In brief, the system was equipped with a Poros A/20 2.1 mm ID x 30 mm column (Applied Biosystems, Foster City, CA, USA) and the flow rate was maintained at 1 mL/min with an injection volume of 50uL. Load/wash buffer solution of 25 mM phosphate with 300mM sodium chloride (pH 7.2) was used in conjunction with a 10 mM glycine elution (pH 3.0) and 10 mM glycine strip buffer (pH 2.5).

2.3. Computational Fluid Dynamics, CFD.

CFD is a very powerful design tool which provides insight into flow patterns, local liquid velocities and local specific energy dissipation rates throughout the agitated flow. Here, the commercial flow solver, Star CCM+ (CD-adapco), was used to predict the internal flows within a single ambr bioreactor operating with 15 ml of media, which corresponds to its maximum fill height, particularly pertinent to operating in the fed-batch mode. It is agitated by the 2- blade impeller designed for it with a swept diameter of D = 11.4 mm; a picture of

the actual blades is shown in Fig. 1bi. The rotational speed of the impeller was set as 1500 rpm (the maximum normally available) and the physical properties of the liquid were taken as water. In these simulations, the RANS realizable two-layer k-ε turbulence model has been selected and applied across the whole flow domain. The realizable k-ε model is substantially better than the standard k-ε model for many applications and when implemented with the two-layer wall treatment allows the use of fine meshes which can resolve the viscous sub-layer. The software allowed the CAD geometry supplied by the manufacturers of the ambr (TAP Biosystems, Royston, Herts., UK) to be directly imported and meshed. Thus the geometry that was simulated is exactly that used to manufacture the ambr bioreactors. The motion of the impeller was represented by a moving reference frame (MRF), comprising an inner mesh that rotates with the impeller and an outer mesh that is stationary with respect to the external walls of the ambr vessel. The two mesh regions are shown in Fig. 2: the inner and outer meshes comprise 0.9 M and 1.5 M cells, respectively; the details of the gas sparger, impeller support pin, shaft and sensor mounting positions are all represented in the raw geometry files imported from the CAD drawings and are fully meshed in the simulations. All solid walls are represented by no-slip boundary conditions and the free surface is specified with a slip (zero-shear stress) boundary condition. Planar sections have been defined within the flow domain, for the display of velocity vector and turbulence dissipation rate fields; these are shown later for vertical and horizontal planes that cut through the centre of the impeller region. Steady-state MRF simulations were run until the normalised residuals were less than 10^{-3}, which required approximately 2600 iterations starting from stationary velocity fields.

2.4. Power, power number, *Po* and mean specific energy dissipation rate, *P/V*.

The power input into the medium can be determined experimentally by a number of techniques [13], all of which are difficult to apply accurately at the very small scale of the

ambr. Here, power measurement was performed on a specially-built stand-alone ambr bioreactor vessel as used in the workstation. In addition in order to assess the impact of the ambr vessel shape and the lack of baffles compared to the usual circular cross-section with baffles, measurements were also made in a cylindrical vessel of 26.0 mm diameter with either two or four 2.6 mm baffles. Measurements in the special ambr vessel were made with fill volumes of 13 mL and 15 mL.

The power number, *Po*, of the impeller is defined as

$$Po = P/\rho N^3 D^5 \qquad 1$$

where P (W) is the power input into the fluid from the impeller, ρ (kg/m^3) is the fluid density, N (rev/s) is the impeller speed and D (m) is the impeller swept diameter. In the turbulent region ($Re = \rho ND^2/\mu > \sim 2 \times 10^4$ [14] where μ (Pas) is the dynamic viscosity) is independent of *Re* and for impellers of the general shape of that in the ambr, it then typically rises very slowly with decreasing *Re* values. Clearly, if *Po* is to be determined accurately, the power input must also be measured with precision.

In each case, the power demand was measured using a small d. c. electric motor (RE-max 17 series, Maxon, Switzerland) directly coupled to the impeller. The motor was carefully chosen to minimise resistive losses and therefore minimise heating in its windings, which would change its resistance and therefore create experimental error if not taken into account. The motor's terminal resistance was measured using a digital multimeter and checked against the manufacturer's specification data sheet. Stirrer speeds from ~ 1500 rpm to ~5500 rpm could be obtained by varying the applied voltage, this speed range being above the normal operating range in order to maximise the power imparted to the fluid relative to the losses, thereby increasing the accuracy of the *Po* determination. At each speed, the power draw was

obtained by measuring the voltage and current to the d. c. motor using digital multimeters with water in the ambr vessel; and with it empty to determine the frictional losses. Current was averaged over a 1 minute period. Impeller speed was measured optically by placing a reflective patch at the top of the impeller shaft and using a hand held tachometer (Veeder-Root).

The large exponent on D in Equ 1 requires the diameter to be defined very precisely. The strict definition is the swept diameter and that is indicated for the ambr impeller in Fig. 1bi. As can be seen the two impeller blades set at 45° to the horizontal are elongated in the vertical direction to maximise their area for their diameter in the small space available, thereby potentially increasing the power input and hence the rate of oxygen transfer and improving blending. In doing so, the impeller appears strictly circular in plan view. To check this assumption regarding the impact of blade shape, it was also decided to measure *Po* for a semicircular blade (Fig. 1bii) which gives the same swept diameter (11.4 mm) but in plan view the projection is an ellipse with the minor axis < 11.4 mm.

The power imparted by the impeller to the fluid, P (W), was calculated from the relationship:

$$P = P_M - P_R - F \qquad 2$$

where P_M is the power to the motor (W), P_R is the loss due to electrical resistance (W) and F is the frictional loss (W). The loss due to the electrical resistance is calculated from:

$$P_R = I^2R \qquad 3$$

where I is the current to the motor (amps) and R is the terminal resistance to the motor (ohms). The frictional loss, F, was found by running the stirrer over the same speed range with the vessel empty and assuming the power required to stir the air was negligible. Thus, P in Equation 2 is equal to zero, which therefore allows F to be calculated. Once the power

to the impeller was found, *Po* was determined for each speed from Equation 1. Finally, the specific power or mean specific energy dissipation rate, *P/V*, could be obtained from,

$$P/V = Po\rho N^3 D^5/V \qquad 4$$

When sparged, an up-pumping agitator loses very little if any power even in bacterial fermentations when the high aeration rate is introduced directly under the impeller, which then effectively disperses the air [10]. Here, the gases are not introduced directly under the impeller, though there is some dispersion, and the sparge rate is very low (at the speeds and flow rates normally used, the gas flow number, Q_G/ND^3 = ~ 6 x 10^{-4}). Therefore, it has been assumed that the unaerated *Po* would apply to the aerated cases to give equivalent power and specific power values too.

2.4. Measurement of k_La

The volumetric mass transfer coefficient k_La was determined at 37 °C in water to aid comparison with the literature, and in the same complete cell culture medium as that used for the cell culture runs plus antifoam (40 µL of 1% Sigma antifoam C). The latter was essential to prevent uncontrolled foaming when sparging. The technique adopted was the static gassing out method [15] with dissolved oxygen being measured from ~ 0% to ~ 100% by using the optical sensor (time constant based on the manufacturer's data of ~ 18 s (PreSens GmbH, Germany)), attached to the bottom of the ambr vessel. Initially, the ambr vessel was agitated and nitrogen was sparged via the sparge tube until the dO_2 reached less than 5 %. Then the agitation and N_2 sparge was stopped, the bioreactor vessel cap was removed and the headspace was gently purged with about 300 ml of air, the whole operation taking less than 10 seconds. Then, air sparging and agitation was started at a set flow rate and stirrer speed and the dissolved oxygen was then recorded every 8 to 20 seconds until the dO_2 reached

100%. To calculate k_La the following equation was used:

$$k_L a(t - t_o) = \ln(100 - C_o / 100 - C) \qquad 5$$

where 100 and C_o are the percentage of dissolved oxygen recorded at saturation and at the time t_o (corresponding to the lowest value of C used from the dynamic response) and C is the percentage saturation at time t (with values up to 80% dO_2). This equation is based on the no-depletion model [16] but since so little oxygen is absorbed in these tiny bioreactors, the method is quite accurate. Also, since the time constant of the dO_2 sensor is << $(k_La)^{-1}$, the dynamics of the sensor may be neglected [17].

k_La was determined at impeller speeds from 300 – 1500 rpm (normal range 1000 to 1500 rpm) with sparged aeration rates from 0.1 – ~ 1.0 mL/min (normal range up to ~ 0.45 mL/min with nitrogen or air at about 0.1 mL/min then supplemented with oxygen to enhance the driving force) with fill volumes of 13 and 15 mL. In addition, measurements were made without sparging in order to get some indication of the contribution of oxygen transfer into the medium through the upper gas-liquid interface.

2.5. Mixing time

The mixing time for an ambr vessel was determined visually over the impeller range 400 – 1500 rpm (normal range 1000 to 1500 rpm) using the starch-iodine decolourisation reaction with sodium thiosulphate [18]. Fill volumes of 13 and 15 mL were used containing the iodine solution with starch added to give a dark blue colour and then 1 mL sodium thiosulphate was added to decolourise it. A timer was started as soon as the sodium thiosulphate was added to the top (as in normal operation); and stopped as soon as complete decolourisation was observed. Video pictures were also taken. Measurements whilst sparging were not

undertaken.

3. Results

3.1. Cell culture in the different bioreactors

A series of reproducible fermentations was carried out with an IgG4-expressing CHO-cell line in the shake flasks, the 5 L Sartorius bioreactor and an ambr system with a commercially available growth medium and feed. The pH for the ambr vessels and 5L bioreactors was maintained at pH 6.9 for the duration of culture, the variation assessed by off-line analysis to be $< \pm 0.05$. Not unsurprisingly, off-line analysis also showed that the shake-flask cultures experienced much larger pH variations, ranging from pH 7.4, at the start of culture, to pH 6.7 during the rapid growth phase (data not shown). dO_2 was controlled at 50% saturation in both the ambr system and the 5 L bioreactor but without control available, it fluctuated in the shake flask with the actual range of values being unknown. The growth profiles for ambr and the 5L bioreactors were quite similar (Fig. 3a), reaching a maximum viable cell density at day 11 with values of 1.4×10^7 and 1.1×10^7 respectively. On the other hand, the cell viability was lowest in the shake flasks (0.8×10^7 cells/mL) and there was a shorter stationary phase at the start of culture. The cell viability remained high in each case (>95%) until day 11 with the ambr and the 5 L bioreactor; but was somewhat lower in the shake flask until day 10 when it then fell away quite rapidly (Fig. 3a). IgG4 production (expressed as % of that obtained with the Sartorius bioreactor), starting at day 6 of culture was very similar for both the 5L bioreactors and the ambr vessels (Fig. 3b). Somewhat surprisingly given the lower cell density and viability, product titre was higher in the shake flasks at some 120 % of that in the ambr and 5L bioreactor at the end of the 18 day culture. Recently industrial users of the ambr system, Amgen [19], Takeda [20], OncoMed [21] and Genentech [22] (in a particularly extensive and detailed study) have also reported that the ambr gives a performance that is a

better indicator of that at the large scale than other scale-down systems. The similarity in biological performance between the ambr and the 5L Sartorius bioreactor in this study is further support for the earlier findings and it is therefore valuable to also establish the physical aspects of the ambr to see how much the physical characteristics mimic those of the larger scale.

3.2. Flow regime

It is important to characterise bioreactors with respect to the organism that it is intended to grow. In particular, cells with low oxygen demand, such as animal cells, require lower specific power inputs than other types of cell. Thus, during the successful cultivation of the CHO cells in the work discussed above, the agitator speed utilised was 1200 rpm in the ambr whilst that in the 5 L Sartorius was much lower at 250 rpm. This reduction in rotational speed is typical of the outcome of scale-up when matching tip speed, as here, or the mean specific energy dissipation rate (equivalent to specific power input) [12]. The flow regime is best defined by the Reynolds number, *Re*; and in the medium used for animal cell culture, these physical properties are similar to water. At the equal tip speeds used during cultivation (equivalent to 250 and 1200 rpm for the 5 L bioreactor and the ambr respectively), the values of *Re* are ~ 1.2×10^4 for the 5 L bioreactor and ~ 2.6×10^3 for the ambr. This reduction of *Re* on scale-down is also quite usual [12] but generally the value is still above 2×10^4 so that the flow is turbulent [23]. Here, whilst in the 5L bioreactor the flow regime is essentially turbulent, that in the ambr is transitional. This lack of similarity with respect to flow regime is inevitable in many ultra scale down studies and the smaller the scale, the greater the disparity. Most design correlations and scaling rules for important physical quantities such as mixing time and oxygen transfer rate have been quantified for the turbulent conditions, hence the change of flow regime on scale-down suggests certain challenges when using such high

throughput equipment.

3.3. Simulation of the ambr flows using CFD

The transitional flow regime poses problems for CFD since ideally the analysis involved requires that the flow be fully turbulent or fully laminar. Here, at 1500 rpm, *Re* = 3250 and so the flow regime was closer to turbulent and was assumed to be so.

The single phase flow simulations obtained from CFD can be used to predict the power number of the ambr impeller by two methods: (1) from a volume integral of the energy dissipation rate and (2) from a torque balance on the rotating impeller blades (or equivalently from the moment acting on the walls of the ambr vessel). The torque balance is obtained by integrating the moments resulting from pressure and viscous shear forces acting on surface of the impeller shaft and blades.

RANS models using the k-ε scheme are known to under predict the magnitude of turbulence in stirred vessels [24], often by as much a 50%. Nonetheless, the mean velocity vector fields are known to be rather well predicted. A volume integral of the turbulence dissipation rate is predicted by CFD to give a specific power input of 230 W/m^3, yielding a power number of 1.15. In contrast a torque balance on the rotating impeller results in a specific power input of 393 W/m^3, yielding a calculated power number of 1.96. Approximately 20% of the torque acting on the impeller results from viscous shear forces, and the remainder from pressure differences around the blade surfaces.

Fig. 4a and 4c show the velocity vector maps and flow patterns on vertical and horizontal planes that cut centrally through the ambr impeller. Fig. 4b and 4d show the distribution of the local specific energy dissipation rate on the same two planes. The tip speed for this simulation is $V_{tip} = \pi ND = 0.90$ m/s, which is the upper end of the colour bar on the figure for

these simulations. The impeller features up-pumping 45° pitched blades and Fig. 4a shows a mixed (radial + axial) component flow leaving upwards; on the right-hand side of Fig. 4a. the discharge impinges on the gas sparge tube and wall and is deflected downwards to form a circulation loop. On the left-hand side, the discharge flow interacts with the relative weak circulations above the impeller and forms an approximately radial outflow. The latter impinges on the left-hand wall and is deflected downwards. The flows in this lower region of the vessel have velocity magnitudes which are less than $V_{tip}/2$ with a strong radial inflow towards the axis of the impeller on the base. In the upper parts of the vessel, the normalised velocities are much lower ($< V_{tip}/10$), with very low normalised velocities close to the free surface. These normalised velocities are very typical of those found with pitched blade impellers as used here in standard vessels in the up-pumping mode [25]. However, because the rotational speed is 1500 rpm (scale down at approximately constant tip speed), the absolute fluid velocity at $V_{tip}/10$ is rather high at ~ 0.9 m/s in such small vessel.

Fig. 4c shows that the region of strong tangential flow is only obtained within the impeller swept volume and hence the proximity of the walls and the gas sparge tube means that this flow is effectively baffled. On the central plane of the impeller the flows outside the boundary of the MRF interface are relatively low especially at the bottom right corner of the ambr vessel. Overall, the flow pattern is very similar to that found under turbulent conditions in traditional baffled configurations using 'elephant ear' impellers which are popular in the large scale cultivation of animal cells [28].

Figs. 4b and 4d show the dissipation rate distribution for the CFD predicted flows; note that the colour bar has a logarithmic scale. The following discussion looks at the order of magnitude of the dissipation rate, bearing in mind the known deficiencies of the RANS k-ε model in predicting turbulence levels and the assumption that the flow is fully turbulent (as

discussed previously it is transitional, *Re* = 3250). In the majority of the impeller swept volume, the local dissipation rates are less than 10 W/kg (equivalent to ~ 10^4 W/m^3) compared to the volume-averaged 230 W/m^3 for the whole vessel. In much of the bulk of the flow, the local dissipation rates are less than 100 W/m^3 and in the corners and close to the free surface the dissipation rate is only about 1 W/m^3, indicating that at this maximum fill height there are regions that are only weakly turbulent. Again, the upper region of the flow, above the upper limit of the blades, exhibits low dissipation rates and low velocity magnitudes.

3.4. Power measurement

Though it is helpful to run at the highest possible speeds in order to keep power losses to an acceptable level, the maximum should be less than that causing headspace gas entrainment as this can dramatically reduce *Po* [27]. Operating the ambr at maximum fill, air ingestion occurred at about 5500 rpm. At that speed, the friction plus electrical resistance losses were less than 10% of the power input into the liquid whilst at 1500 rpm, close to the maximum normal operating speed, losses up to 50 % occurred. Fig. 5 shows *Po* vs *Re* for this speed range for both the ambr impeller and vessel (Fig. 1bi) and the semi-circular blades in the ambr vessel (Fig. 1bii). Similar data are shown for measurements in the baffled circular cross section vessel. For the ambr impeller and vessel configuration, *Po* was ~ 2.1 and essentially the same value was found for the ambr impeller in the circular vessel independent of the number of baffles (the results are only shown for 4 baffles, although 2 baffles were also studied). This similarity suggests that the combined ambr vessel and impeller configuration provides effective baffling. For the semi-circular 11.6 mm blades (Fig. 1bii) in the ambr vessel, *Po* was 20% lower at ~ 1.7; and lower again at ~1.5 in the circular one. This difference shows the effectiveness of extending the blade length to enhance the power input to improve mixing processes. For the ambr impeller, the two lower fill heights were also used

and similar *Po* values were obtained (data not shown).

For the maximum fill height, i.e. at the maximum normal working volume of 15 mL, a power number of 2.1 gives a specific power input at 1500 rpm of 420 W/m^3.

3.5. Mixing time

The mixing time is defined as the time taken for all the contents to be mixed so when it is done by a decolourisation technique it is the time for the entire colour to disappear. The advantage of this method is that it gives some indication of the rate of mixing of the different parts of the tank to be assessed. In order to indicate the general way that this occurs, photographs in Fig. 6 illustrating this progression were obtained at 400 rpm, well below the normal operating speed. As can be seen, after addition to the top surface, the bulk of the tank loses colour rapidly indicating good mixing. Nevertheless a fairly thin layer (< ~ 10mm) near the relatively-quiescent zone at the air-liquid interface decolorizes more slowly and this defines the mixing time. Table 1 shows the measured mixing times for all the conditions tested whilst Fig. 7 shows the data in graphical form.

3.6. Volumetric mass transfer coefficient

Tables 2 and 3 give the k_La values for water and medium plus antifoam respectively for fill levels of 13 mL and 15 mL. In all cases, the water values are higher than those with medium. This difference is not surprising since any addition to water tends to have a measureable effect on k_La where typically salts increase it whilst antifoam significantly reduces it (as does Pluronic F68 but to a lesser extent) [16]. However, the k_La values for both are well within the range of those reported for larger scale cell culture (up to about 15 h^{-1}) [2, 28]. In addition, k_La increases with increasing air flow rate, agitation speed and specific power as expected [16 17]. Thus, the k_La is bigger in the smaller volume because the *P/V* is larger for the same

agitator speed. In addition, the results for zero sparging can be considered as the k_La associated with surface aeration. In general, it is very close to the values obtained at the lowest sparge rate. This significant contribution from surface aeration also encourages higher k_La values at the lower fill volume.

4. Discussion

4.1. Power number and specific power input

Here it is shown that the physical characteristics of the ambr are in some important ways quite different from those of larger stirred bioreactors used for cell culture. Most significantly, the mean specific energy dissipation rate utilised during the run (215 W/m^3) giving good biological performance is much higher than that normally encountered at the commercial scale. The high values used here are commonly considered to raise concerns about 'shear damage' to cells [23]. On the other hand, they are slightly lower than the values reported (250 W/m^3) to give satisfactory performance with a range of cell lines [2]. Indeed, very recent work [29] has shown equivalent process performance and product quality with two CHO cell lines when agitated by dual Rushton turbines at 1000 W/m^3 compared to those under historical agitated conditions of ~ 20 W/m^3 at both the bench and commercial scale. When viewed this way, the 'good' performance in the ambr does not seem so surprising and further indicates, contrary to perceived wisdom, the robustness of animal cells. In addition, it should be noted that the high *P/V* value is because the tip speed in the ambr was maintained the same as that at the 5 L scale, a common scaling relationship [12]. As set out in the Conclusions, the flexibility of the ambr allows lower *P/V* to be used for holding dO_2 at the desired value.

The CFD predicted power number from a torque balance on the impeller blades and shaft of $Po = 1.96$ compares rather well with the measured average value of $Po = 2.1$ (shown as ambr

14.8 mm blades in Fig. 5); the error compared to the experimental measurements is only 7%, which seems quite acceptable, considering the difficulties associated with the CFD analysis because the flow is transitional and the power measurement on such a small scale. Previous studies (e.g. Rielly & Gimbun, [24]) indicate that k-ε turbulence models give reasonable predictions of the mean velocity fields and impeller torques. On the other hand, the volume integral of the dissipation rates yields a power number that is only 55% of the experimentally measured value. However, that is consistent with reported under-predictions based on the k-ε approach [24] which are usually attributed to the strong streamline curvature found in stirred vessel flows, along with the strong anisotropy of the turbulence close to the impeller blades [30].

4.2 Mixing characteristics

It is interesting to note that the quiescent zone at the air-liquid interface at the maximum fill height and low impeller speed (outside of the normal operating range) (Fig. 6) fits in well with the CFD analysis of this condition, which shows very low velocities and specific energy dissipation rates in this region (Fig. 4). It is also of value to compare the measured mixing times with correlations in the literature which have been shown to work well for standard (bio)reactor configurations with different aspect ratios for turbulent and transitional flow. In order to do so, it is necessary to estimate a vessel diameter, T. This can be done by assuming the cross-sectional area, CSA, is the same as a circle of the same area, i. e.

$$T = \sqrt{\frac{4 \times CSA}{\pi}} = \sqrt{\frac{4 \times 0.028 \times 0.015}{\pi}} = 0.023 \text{ m} \qquad 7$$

For the liquid fills of 13 and 15 mL, the fill heights are 31 and 36 mm respectively to give aspect ratios of 1.35 and 1.57. For flow in the transitional flow regime (as found here) for *Re*

< $6400Po^{-1/3}$ (which for the ambr impeller means Re < 5000; here the maximum is ~3.2 x 10^3), the mixing time for an aspect ratio of 1 can be estimated [14] from,

$$N\theta_m = 3.4\times10^4 Re^{-1}Po^{-2/3}\left(\frac{D}{T}\right)^{-2} \qquad 8$$

For the maximum agitator speed of 1500 rpm, Equ. 8 gives a time of 1.1 s. For an aspect ratio of > 1, the mixing time increases under turbulent conditions by $(H/T)^{2.43}$ which, if it is assumed that the relationship applies to transitional flow, for the highest aspect ratio increases the time to 3.1 s. The actual measured time is 5 s. Thus, although a number of assumptions have been made, these calculations indicate that the equations for the mixing time in the literature for the transitional regime give an approximate estimate of those found in the ambr.

Somewhat surprisingly, however, Fig. 7 shows that the data overall give a satisfactory fit to the mixing time functionality found in the turbulent regime, namely $\theta_m N$ = constant for each of the two fill levels. However, the calculated values of mixing times from the equations for the turbulent regime [14] give values much smaller than the experimental (data not shown). Overall, the experimental times are of the order to be expected in bench scale stirred bioreactors that operate in the turbulent regime [6], though they are considerably lower than those found on the plant scale [2].

4.3. Volumetric mass transfer coefficient, k_La

There are a very large number of correlations available in the literature for estimating k_La for sparged systems but the two equations developed from a survey of the literature by Van't Riet [17] are commonly used as bench marks. The equations were of the form,

$$k_L a = A\left(\frac{P_g}{V}\right)^a (v_S)^b$$

where for coalescing systems (mainly based on studies with water), A = 2.6 x 10^{-2}, a = 0.4 and b = 0.5 when the units of k_La are s^{-1}, of P_g/V, W/m^3 and of v_S, the superficial gas velocity, m/s. For non-coalescing systems (mainly based on electrolyte solutions) which have smaller bubbles, generally leading to higher k_La values compared to water, the constants A = 2 x 10^{-3}, a = 0.7 and b = 0.2. Though these equations were based on higher agitation intensities ($500 < P_g/V < 10^4$) and much higher sparge rates than those used in animal cell culture, previous work [31, 32] under cell culture conditions found the equations gave reasonable predictions for bench and pilot scale bioreactors. The presence in the medium of antifoam and Pluronic F68, both of which tend to lower k_La (by about a factor of 2) and other components including salts which raise it relative to water (up to about 10-fold) [16], makes it very difficult to predict absolute values; or to predict which equation will give the better fit (if any). Calculating the superficial air velocity, v_S, from the volumetric flow rate based on the estimated ambr vessel diameter of 23 mm gives a maximum v_S of ~ 5 x 10^{-5} m/s. Assuming for the reasons explained earlier, $P_g = P$, the unaerated value, based on the torque measurements, the maximum P/V is ~ 420 W/m^3 for the 15 mL fill level, the calculated values for k_La are 2.05 x 10^{-3} s^{-1} (= 7.4 h^{-1}) and 0.019 s^{-1} (68 h^{-1}) for the coalescing and non-coalescing cases respectively. Clearly at this scale in this mixture of medium and antifoam, k_La in water and in the medium are much closer to each other than the literature would suggest, both being similar (Table 2 and 3) to the value predicted from the correlation of Van't Riet [17] for coalescing conditions. This result is in agreement with the bench scale work of Lavery and Nienow [31] with the enhancing effect of the salts and the reduction caused by the antifoam plus Pluronic F68 balancing out each other.

Recently, an equation for k_La in a representative culture medium including Pluronic F68 and

antifoam based on measurements from large scale bioreactors has been published with A = 0.075, a = 0.47 and b = 0.8 [28]. This equation predicts a maximum k_La of 1.7 h^{-1} much lower than the values found here (Tables 2 and 3). Clearly, a wide range of values can be predicted based on equations in the literature; but even those which have used an apparently similar liquid phase composition cannot be used with confidence as a means of predicting k_La at this small scale because of the huge differences in *Re*, scale and superficial gas velocity.

Therefore, it is interesting to find a good fit to the data in the Tables, both for water and the present medium plus antifoam, using an equation of the form of Equ. 8 but with units that relate to the conditions generally used for cell culture at this scale and for ambr in particular. To make this assessment, it would also be useful to have the correlation in terms of agitator speed and flow rate in mL/min as they are the parameter that are easily set on the ambr workstation. Recognising that for each fluid, the exponent on speed, *N*, should be 3 times that on *P/V* and that on air flow rate should be the same; and that two different equations should be required for the two fill levels when expressed in terms of *N* but only one when expressed as *P/V*, by graphical inspection, it was seen that exponent on *P/V* of 0.3 and on *N* of 0.9 together with an exponent on airflow rate in mL/min of 0.15 all gave good fits (see Table 4). The difference between the R^2 values for the exponents chosen and those for the best fits are never greater than 0.01. This way of expressing the data also enables the small difference between water and medium and between the two fill levels to be easily seen. Finally, a parity plot for all the k_La data in the medium based on the units and constants used for Eq 3 in Table 4 is shown in Fig 8. Of course, the actual k_La values obtained in any particular application will depend on the precise composition of the medium (including Pluronic F68) and the amount and type of antifoam used.

An inspection of the data in Tables 2 and 3 shows that in every case, k_La without sparging is

very similar to that at the lowest sparge rate. As the scale gets smaller, the specific surface area available for mass transfer gets greater; for geometrically similar systems, it is inversely proportional to the bioreactor diameter. In the case of the ambr, it is greater for the 13mL fill than the 15 mL. As a result, there is a large contribution from surface aeration across the range of conditions used, so that the k_La is a little higher even at the same specific power at the 13 mL fill level compared to the 15ml (which is contrary to the implications of Equ. 9 and increases the scatter in the data of Fig. 8 and increases the value of R^2 for the k_La correlations based on *P/V* for the present results). In addition, it explains why the exponent on both superficial velocity and specific power is low compared to the correlations of Van't Riet [17] and others [16] based on measurements in larger scale equipment where the reduced specific surface and the higher superficial gas velocities make the contribution of surface aeration negligible.

It is also interesting to consider the values of *P/V* and air flow rate giving rise to the present k_La values compared to those found at the commercial scale. Firstly, most of the *P/V* values are much higher than those normally used in animal cell culture (up to ~ 50 W/m^3 is typical [2]). However, the situation in relation to air sparging is more complicated. Though the air sparge rate under normal conditions (0.15 mL/min) is similar to that used at the larger scale when expressed as vvm (0.01 vvm), it becomes higher with the additional oxygen flow required to give the desired driving force and hence dO_2, which increases the flow rate to 0.45 mL/min (~ 0.03 vvm). This increased vvm flow helps carbon dioxide stripping [2] and pCO_2 control [33]. However, in terms of superficial air velocity (important for k_La), the flow is very low (maximum ~ 2 x 10^{-5} m/s), which also encourages a significant contribution from the upper surface to the overall rate of mass transfer at this scale as can be seen in Table 2 and 3. Also, at such low superficial air velocities, relatively high *P/V* values would be

required to maintain a sufficient rate of oxygen transfer using that parameter and air flow rate only to maintain the correct dO_2. By sparging oxygen to increase the driving force (and gas velocity) the ambr system controls dO_2 whilst limiting the specific power, though it is still higher than at the larger scale. These differences provide a good example of the changes that can arise when the variation of scales is very significant, with the control strategy employed in the ambr still effectively maintaining the critical process parameter (dO_2) at the required level.

4.4. Biological considerations

Since shake flasks and the ambr system are both intended to be used at an early stage for clone selection and as an indicator of performance at the large scale, it is interesting to note that the shake flask performed differently to the stirred ambr and 5L Sartorius bioreactors. These differences may simply be due to a lack of an adequate pH or dO_2 control strategy in the shake flasks as compared to the relatively tight control in the stirred systems. Indeed the shaken system used here has a very primitive control strategy for pH *via* a CO_2/bicarbonate buffering system, which whilst effective for gross pH control does mean that fine control is lost. For the stirred systems, the same buffering system is augmented by increasing or decreasing the rate of CO_2 gassing and by the introduction of additional sodium bicarbonate on demand. In this way, growth medium pH control is achieved with much more accuracy. It is known that a cell exerts very tight control of its internal cytoplasmic pH [34]. In most organisms, the internal pH varies by only 0.1 unit per pH unit change in external medium pH. The ability to regulate internal pH in such a way implies control over the permeability of the cytoplasmic membrane to protons, achieved *via* energy-dependent ion transport systems [35]. Therefore in a shake flask cells may be expending energy maintaining intracellular pH rather than producing more cells.

The dO_2 and pCO_2 in shake-flasks is controlled by passive diffusion of oxygen into the liquid through the headspace, with no control over the mass transfer itself other than through the fixed orbital speed. For the ambr and 5L bioreactors, although the impeller speed and nitrogen flow rates were fixed, the dO_2 was controlled by varying the oxygen flow rate through the sparger, and hence the total flow rate and the driving force. It is possible that oxygen transfer rates in shake-flasks were so low that oxygen limitation occurred and it is known that imposing such an environmental stress on the cell can lead to lower cell numbers and higher protein yields [36]. Indeed, in the more extensive study of the biological aspects by Hsu et al.[22], in 3 of the 4 cell lines studied, the protein yield was on average ~ 20% greater in the uncontrolled environment of the shake flask.

Finally, it is interesting to speculate why, compared to other systems for rapid screening, the biological performance is so similar in the ambr and other stirred bioreactors across the scales, as seen in this study and in a number of other recent papers and conference presentations, given the notable differences in the physical environment. It may be that cells respond in an integrated way to a combination of stresses from fluid mechanical processes (in the bulk of the agitated broth and from bursting bubbles) and environmental experiences (variation with respect to nutrient concentration, pH, dO_2, pCO_2, or osmolality). In all cases, the fluid mechanical stresses are generated in the same way (stirring and sparging) but they are greater at the ambr scale, although as is shown here and elsewhere [7, 23], this has no effect on cell viability or biological performance. On the other hand, the environmental stresses are greater at the larger scales as the homogeneity deteriorates with increasing scale [2]. The overall result is similar performances with respect to viable cell density and product titre.

5. Conclusions

A series of reproducible fed-batch fermentations was carried out with an IgG4-expressing CHO-cell line in a 5 L Sartorius bioreactor, 250 ml shake flasks and an ambr system (at a fill volume of 15 ml) with a commercially available growth medium and feed. In each type of bioreactor, satisfactory cell growth was achieved but the performance in the Sartorius bioreactor and ambr were quite similar to each other and rather different to that found in the shake-flask. These findings accord well with recent reports that the biological performance of the ambr gives a better indication of the performance in larger scale stirred bioreactors than shake flasks [19, 20, 21, 22].

However, for the first time, the physical characteristics of the ambr have been studied in depth. Such characterisation is particularly important as in earlier work [22] using the standard ambr system, where although the wide-ranging biological comparisons made were sound, the power number of the ambr impeller was incorrectly taken as 0.6 and its diameter as 11 mm. As a result, the specific power input for the ambr was underestimated by a factor of 4.2 and so the similarity claimed for the specific power at the ambr and 5L bioreactor scale in that study was also incorrect. Here, a much more accurate estimate of power number has been presented, and it is shown that there are a number of physical features which are quite different in the ambr compared to those found at the larger scale. This difference is largely related to the very small scale of the ambr; this leads to Reynolds numbers in the transition region and very low superficial gas velocity, $v_{S,}$ for the sparged gas. The change of flow regime does however lead to mixing times comparable with those found at the bench scale, supporting scalability of biological performance. Also, since the k_La required to meet the oxygen demand depends on v_S, the very low value of the latter requires significantly higher mean specific energy dissipation rates than would normally be imposed. However, this

increase in specific power is limited by employing a dO_2 control strategy which involves increased rates of oxygen sparging, which increases the driving force and k_La, thus supporting scaleable biological performance. Indeed, given the flexibility of the ambr control system, it is possible to control the dO_2 to the desired level via the oxygen flow rate to adjust the driving force; and via that and the agitator speed (the specific power) to adjust the k_La whilst still maintaining adequate blending.

However, the finding that, at the control settings used here giving high specific energy dissipation rates, the cells grow well is in agreement with other controlled studies extending over many years showing the robustness of animal cells [7, 29] despite a widespread perception based on their size and lack of cell wall that they are very ‘shear sensitive’.

Nomenclature

A,a,b	Constants
C	Percentage O_2 saturation
CSA	Cross-sectional area of vessel
D	Impeller diameter
F	Power required to overcome friction
H	Liquid height in vessel
I	Current to the motor
k_La	Specific volumetric mass transfer coefficient
N	Impeller speed
Po	Power number
P/V	Mean specific energy dissipation rate or specific power imparted to the fluid
P_M	Power to the motor
P_R	Power loss due to resistance in the motor
P_g	Power input form impeller when sparging
Q_G	Volumetric gas flow rate
R	Terminal resistance to the motor
R^2	The square of the sample correlation coefficient
Re	Reynolds number
t	Time
T	Vessel diameter
V	Volume of fluid in the bioreactor
v_s	Superficial gas velocity
V_{tip}	Impeller tip speed
μ	Dynamic viscosity
ρ	Density
θ_m	Mixing time

Subscript

o	At the start of the measurement of k_La

Abbreviations

ambr	TAP Biosystems trade mark for its advanced micro-bioreactor
CAD	Computer-aided design
CFD	Computational fluid dynamics
HPLC	high pressure liquid phase chromatography
k-ε	Description of turbulence model used in CFD
MRF	Moving reference frame
RANS	Reynolds average Navier-Stokes
vvm	volumetric gas flow rate per volume of reactor

Acknowledgements

The authors would like to acknowledge Lonza Biologics (Slough, UK) for providing the model CHO-cell line. Additionally the authors would like to acknowledge the Technology and Strategy Board (UK) for their financial support.

References

[1] A.J. Want, A.W. Nienow, C.J. Hewitt, K. Coopman, Large-scale expansion and exploitation of pluripotent stem cells for regenerative medicine purposes: beyond the T flask, Regen. Med. 7 (2012) 71–84.

[2] A.W. Nienow, Reactor engineering in large scale animal cell culture, Cytotechnol. 50 (2006) 9-33.

[3] R. Bareither, D. Pollard, A review of advanced small-scale parallel bioreactor technology for accelerated process development: Current state and future need, Biotechnol. Prog. 27 (2011) 2-14

[4] J.I. Betts, F. Baganz, Miniature bioreactors: current practices and future opportunities, Microb. Cell. Fact. 5 (2006) 1-14.

[5] J. Büchs, Introduction to advantages and problems of shaken cultures, Biochem. Eng. J. 7 (2001) 91-98.

[6] C.J. Hewitt, A.W. Nienow, The scale-up of microbial batch and fed-batch fermentation processes, Adv. Appl. Microbiol., 62 (2007) 105-136.

[7] S.K.W. Oh, A.W. Nienow, A.N. Emery, M. Al-Rubeai, Further studies of the culture of mouse hybridomas in an agitated bioreactor with and without continuous sparging, J. Biotechnol. 22 (1992) 245-270.

[8] T. Anderlei, J. Büchs, Device for sterile online measurement of the oxygen transfer rate in shaking flasks**,** Biochem. Eng. J. 7 (2001) 157-162.

[9] C. Wittmann, H.M. Kim, G. John, E. Heinzle, Characterisation and application of an optical sensor for quantification of dissolved oxygen in shake-flasks, Biotechnol. Lett. 25 (2003) 377-380.

[10] A.W. Nienow, Scale-up, stirred tank reactors, in: M.C. Flickinger (Ed.), Encyclopedia of Industrial Biotechnology, John Wiley & Sons, Inc., Hoboken, NJ, USA, Vol. 7, 2010, pp 4328 – 4341.

[11] M.P.C. Marques, J.M.S. Cabral, P. Fernandes, Bioprocess scaleup: quest for the parameters to be used as criterion to move from microreactors to lab-scale. J. Chem. Technol. Biotechnol. 85 (2010) 1184-1198.

[12] A. Amanullah, B.C. Buckland, A.W. Nienow, Mixing in the fermentation and cell culture industries, in E.L. Paul, V.A. Atiemo-Obeng, S.M. Kresta (Eds.), Handbook of Industrial Mixing; Science and Practice, Wiley-Interscience, N.Y., Ch. 18, 2004, pp 1071-1157.

[13] G. Ascanio, B. Castro, E. Galindo, Measurement of power consumption in stirred vessels—a review, Chem. Eng. Res. Des. 82(A) (2004)1282–1290.

[14] A.W. Nienow, Hydrodynamics of stirred bioreactors, App. Mech. Rev. 51 (1998) 3-32

[15] B. Atkinson, F. Mavituna, Biochemical Engineering and Biotechnology Handbook, 2nd

ed., Stockton Press, UK, 1991.

[16] A.W. Nienow, Aeration-biotechnology, Kirk-Othmer Encyclopedia of Chemical Technology, Fifth ed, Wiley, New York, on-line edition. 2003.

[17] K. van't Riet, Review of measuring methods and results in non-viscous gas–liquid mass transfer in stirred vessels, Ind. Eng. Chem. Proc. Des. Dev. 18 (1979) 357–364.

[18] D.G. Cronin, A.W. Nienow, G.W. Moody, An experimental study of the mixing in a proto-fermenter agitated by dual Rushton turbines, Food. Bioprod. Proc. 72(C) (1994) 35-40.

[19] C. Zupke, D. Ulibarri, J. Wendling, Evaluation of the ambr microreactor system, Cell Culture Engineering XIII, Poster 40, Scottsdale, Arizona, USA, 2012.

[20] M. Carpio, S. Patel, Evaluation and characterisation of the advanced microscale bioreactor (ambr) system for use in antibody cell line development, Cell Culture Engineering XIII, Poster 127, Scottsdale, Arizona, USA, 2012.

[21] C.L. Casipit, J. Burky, R. Townsend, D.L. Traul, N. Sar, P. Stathis, M. Mulkerrin, Advanced microscale bioreactor, ambr, for the rapid screening of biopharmaceutical producing cell lines, Cell Culture Engineering XIII, Poster 38, Scottsdale, Arizona, USA, 2012.

[22] W.-T. Hsu, R.P.S. Aulakh, D.L. Traul, I.H. Yuk, Advanced microscale bioreactor system: a representative scale-down model for bench-top bioreactors, Cytotechnol. 2012, DOI 10.1007/s10616-012-9446-1.

[23] A.W. Nienow, Impeller selection: animal cell culture, in: M.C. Flickinger (Ed.), Encyclopedia of Industrial Biotechnology, John Wiley & Sons, Inc., Hoboken, NJ, USA, Vol. 5, 2010, pp. 2959-2971.

[24] C.D. Rielly, J. Gimbun, Computational fluid mixing, in: P.J. Cullen (Ed.), Food Mixing: Principles and Applications. Chichester, Wiley Blackwell, UK, 2009, pp. 125-174.

[25] Z Jaworski, K.N. Dyster, A.W. Nienow, The effect of size, location and pumping direction of pitched blade turbine impellers on flow patterns: LDA measurement and CFD predictions, Chem.Eng.Res.Des., 79(A) (2001) 887-894.

[26] H. Zhu, A.W. Nienow, W. Bujalski, M.J.H. Simmons, Mixing studies in a model aerated bioreactor equipped with an up- or a down-pumping 'elephant ear' agitator; power, hold-up and aerated flow field measurements, Chem. Eng. Res. Des. 87(A) (2011) 307-317.

[27] W. Bujalski, A.W. Nienow, S. Chatwin, M. Cooke, The dependency on scale of power numbers of Rushton disc turbines, Chem. Eng. Sci. 42 (1987) 317-326.

[28] Z. Xing, B.M. Kenty, Z.J. Li, S.S. Lee, Scale-up analysis for a CHO cell culture process in large-scale bioreactors, Biotechnol. Bioeng. 103 (2009) 733-746.

[29] W.H. Scott, C.R. Thomas, C.J. Hewitt, G. Lewis, S.J. Meier, A. Amanullah, R. Kiss, A.W. Nienow, Scale-down studies for assessing the impact of different stress parameters on growth and product quality during mammalian cell culture, in Proc. 14th European Conference on Mixing, Warsaw University of Technology, Warsaw, September 2012, pp 431 – 436, ISBN 978-83-906658-8-7.

[30] F.R. Khan, C.D. Rielly, D.A.R. Brown, Angle-resolved stereo-PIV measurements close to a down-pumping pitched-blade turbine, Chem. Engg Sci. 61 (2006) 2799-2806.

[31] M. Lavery, A.W. Nienow, Oxygen transfer in animal cell culture medium, Biotechnol. Bioeng. 30 **(**1987) 368-373.

[32] C. Langheinrich, A.W. Nienow, N.C. Stevenson, A.N. Emery, T.M. Clayton, N.K.H. Slater, Oxygen transfer in stirred bioreactors under animal cell culture conditions, Food. Bioprod. Proc. 80(C) (2002) 39-44.

[33] C. Sieblist, O. Hägeholz, M. Aehle, M. Jenzsch, M. Pohlscheidt, Lübbert, A. Insights into large-scale cell-culture reactors: II. Gas-phase mixing and CO_2 stripping. Biotechnol. J. 6 (2011) 1547–1556**.**

[34] I.R. Booth, Regulation of cytoplasmic pH in bacteria, Microbiol. Rev. 49 (1985) 359-378.

[35] H. Onyeaka, A.W. Nienow, C.J. Hewitt, Further studies related to the scale-up of high cell density *Escherichia coli* fed-batch fermentations: the additional effect of a changing micro-environment when using aqueous ammonia to control pH, Biotechnol. Bioeng. 84 (2003) 474 – 484.

[36] S.Tissot, A. Oberbek, M. Reclari, M. Dreyer, D.L. Hacker, L. Baldi, M. Farhat, F.M. Wurm, Efficient and reproducible mammalian cell culture bioprocesses without probes and controllers? N. Biotechnol. 28 (2011) 382–390.

Figure captions

Figure 1a) Diagrammatic representation of the ambr bioreactor and position of the impeller, sparge tube and probes (internal cross-section 28 mm x 15 mm; with a fill volume of 15 mL, the liquid height is 36 mm); 1b) The impellers for which the power was measured showing the swept diameter, D = 11.4 mm: i) the actual ambr impeller with 'stretched' blades at 45° to the horizontal so that the diameter of the minor axis is 11.4 mm and that of the major axis is 14.8 mm, giving a plan view which is a circle diameter, 11.4 mm; ii) an impeller of the same swept diameter with two approximately semi-circular blades to give a swept diameter of 11.4 mm, which in plan view is an ellipse.

Figure 2 The computational mesh generated for the ambr bioreactor, showing the moving reference frame comprising an inner mesh concentric with the impeller.

Figure 3 Biological data for ambr, shake flask (SF), and Sartorius bioreactor (5.0L). Error bars indicate the range of the results obtained: a) Viable cell density profiles; and b) IgG4 titre (as % of that obtained in the Sartorius bioreactor)

Figure 4 CFD simulations showing a horizontal and vertical plane through the centre of the impeller and ambr vessel: (a) and (c) mean velocity vectors and (b) and (d) turbulent specific energy dissipation rate.

Figure 5 Power number v Re for the two different impellers: ▼ ambr impeller in the ambr vessel; Δ ambr impeller in the cylindrical vessel with 4 baffles; • Fig 1 bii impeller in the ambr vessel; o Fig 1 bii impeller in the cylindrical vessel with 4 baffles.

Figure 6 Pictures showing the progress of homogenisation in an ambr vessel with a maximum fill volume of 15ml (Liquid height, 36 mm) at 400rpm (normal operating range

1000 to 1500 rpm).

Figure 7 Mixing time versus agitator speed for 13 and 15 mL fill heights with the best fit line through the data for $\theta_m N$ = constant

Figure 8 Parity plot for $k_L a$ (h^{-1}) correlation ($k_L a = 1.74(P/V)^{0.3}(Q_G)^{0.15}$) for oxygen transfer into the media plus antifoam, in terms of specific power input, P/V (W/m^3) and volumetric air flow rate, Q_G (mL/min) for both 13 mL and 15 mL fills.

Tables

Table 1 Measured mixing times at different agitator speeds and fill levels.

Table 2 k_La (h^{-1}) values with water at different fill levels, air flow rates, agitator speeds and specific power inputs.

Table 3 k_La (h^{-1}) values with medium plus 40 µL of 1% Sigma antifoam C at different fill levels, air flow rates, agitator speeds and specific power inputs.

Table 4 k_La correlations and R^2 for each for the ambr: Eq 1) For water, $k_La = A(P/V)^{0.3}(Q_G)^{0.15}$; both 13 and 15 mL; Eq 2) For medium, $k_La = A(P/V)^{0.3}(Q_G)^{0.15}$; both 13 and 15 mL; Eq 3) For 13 ml medium, $k_La = A(N)^{0.9}(Q_G)^{0.15}$; Eq 4) For 15 ml medium, $k_La = A(N)^{0.9}(Q_G)^{0.15}$. In all cases, k_La is in h^{-1}, N is in rpm, P/V is in W/m^3 and Q_G is in mL/min

Figures

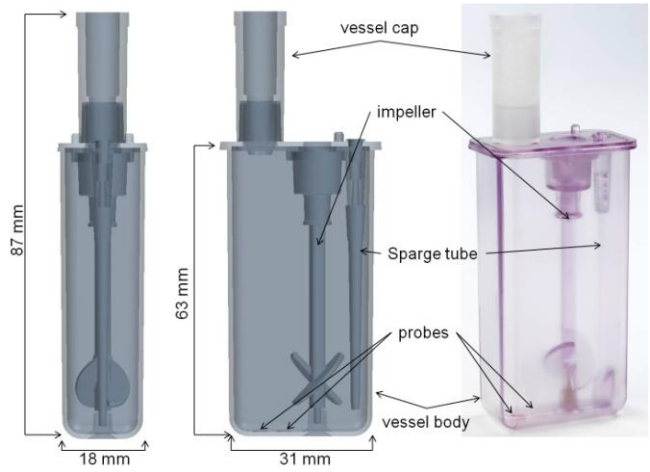

a)

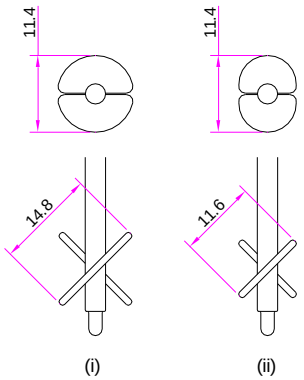

b)

Figure 1

Figure 2

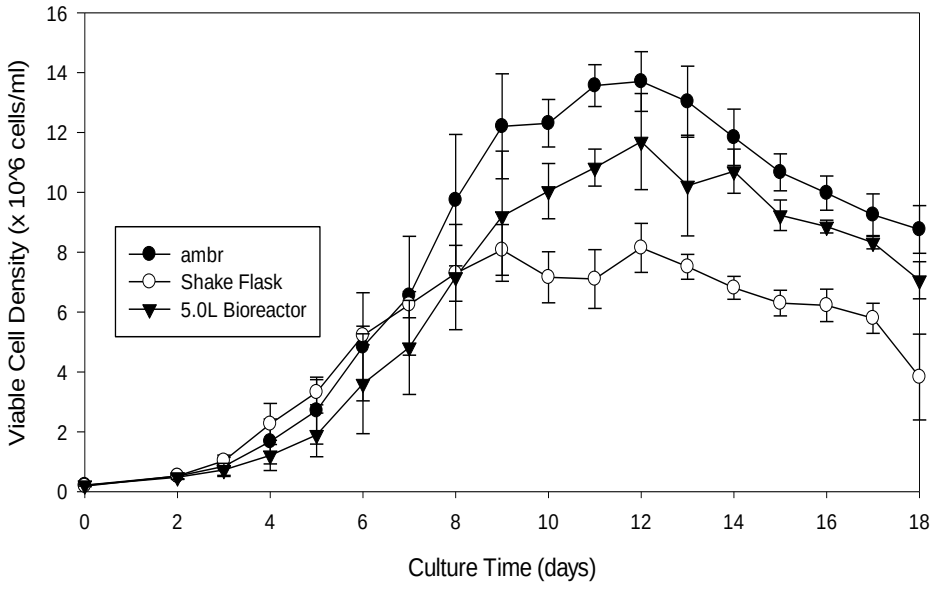
Viable Cell Density (x 10^6 cells/ml)
Culture Time (days)
ambr
Shake Flask
5.0L Bioreactor
0
2
4
6
8
10
12
14
16
18

a)

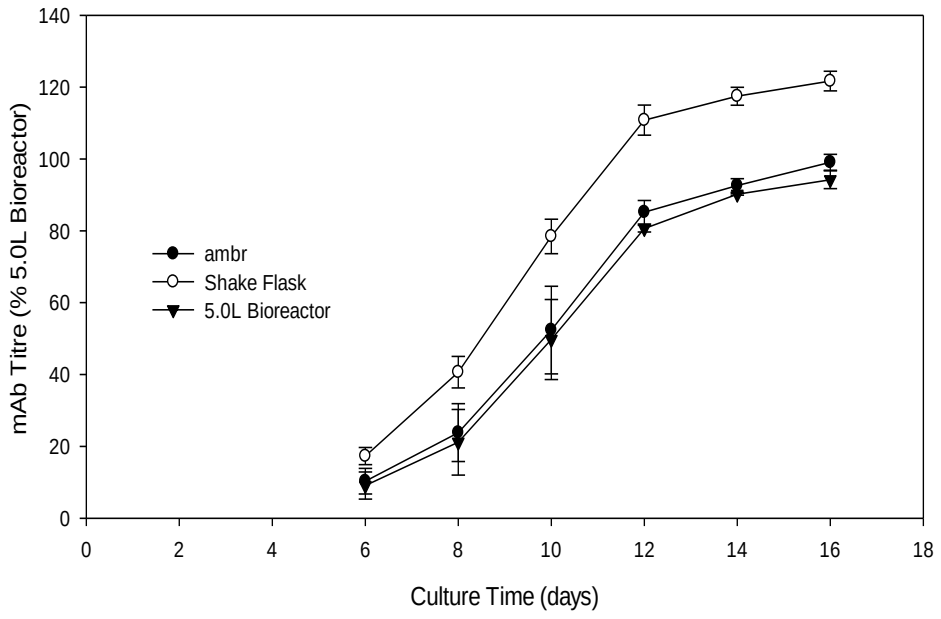
mAb Titre (% 5.0L Bioreactor)
Culture Time (days)
ambr
Shake Flask
5.0L Bioreactor
0
20
40
60
80
100
120
140
2
4
6
8
10
12
14
16
18

b)

Figure 3

a)

b)

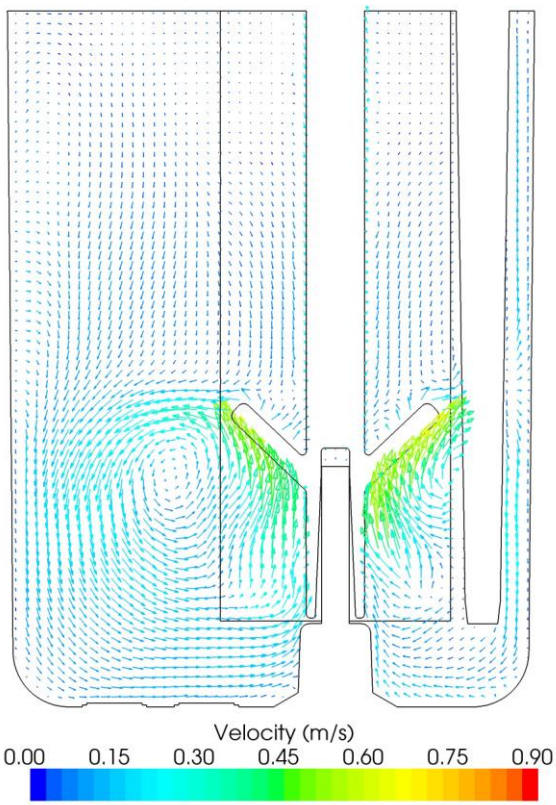

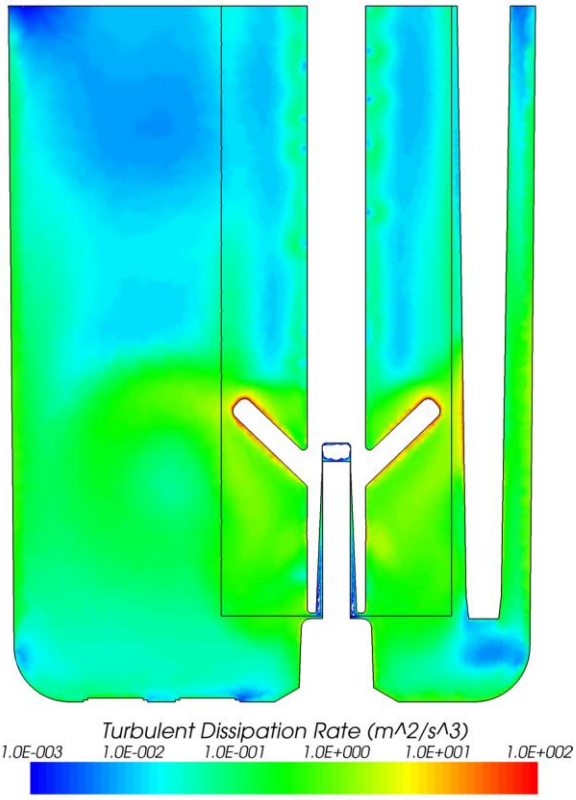

c)

d)

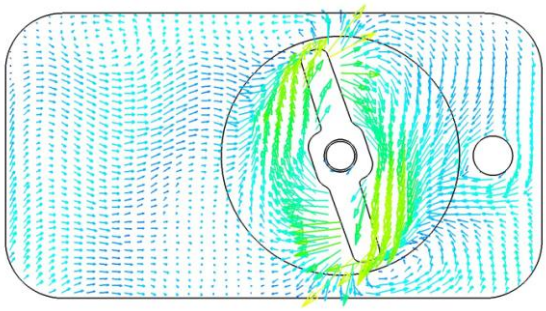

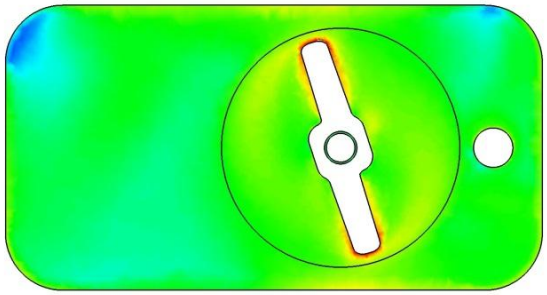

Figure 4

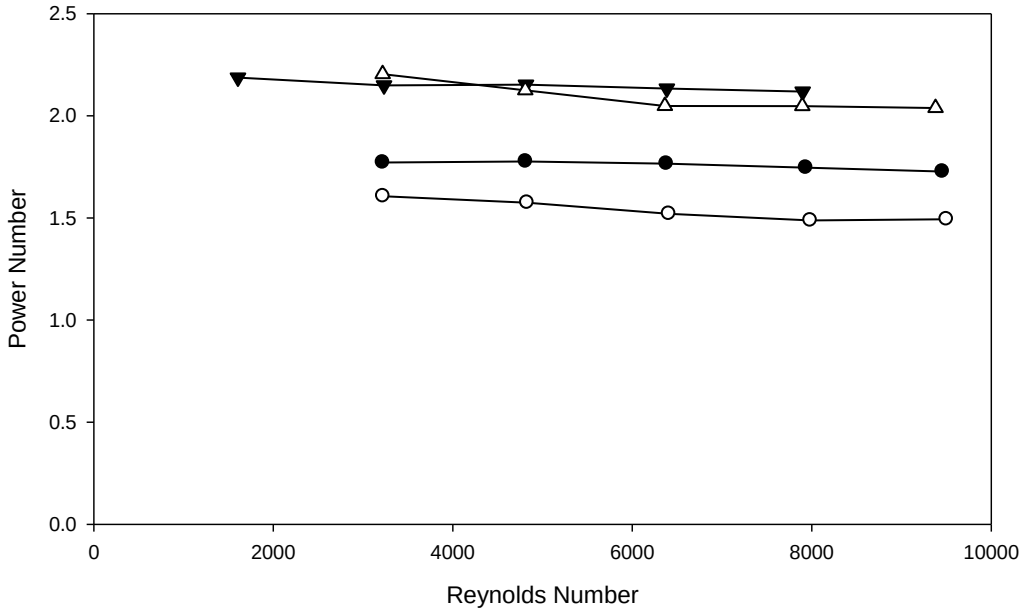

Ambr vessel, 11.6 mm impeller blades
Circular vessel (Dia 26mm), 4 baffles, 11.6 mm impeller blades
Ambr vessel, 14.8mm impeller blades
Circular vessel (Dia 26mm), 4 baffles,14.8 mm impeller blades

Figur

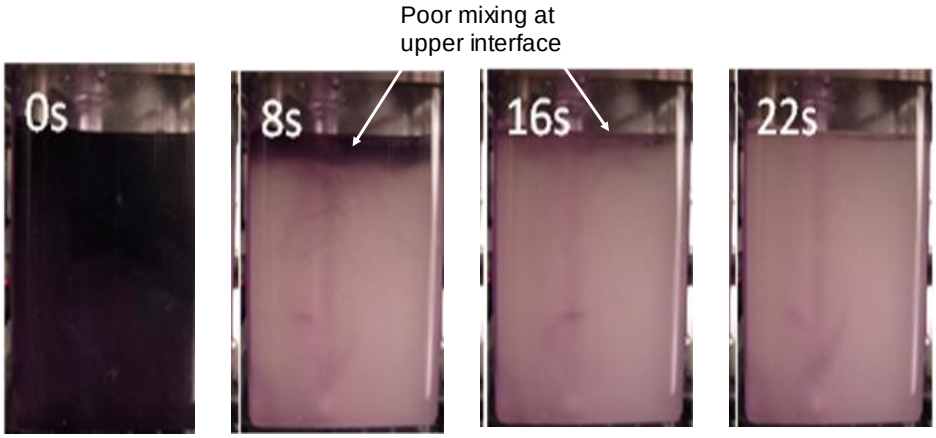

Figure 6

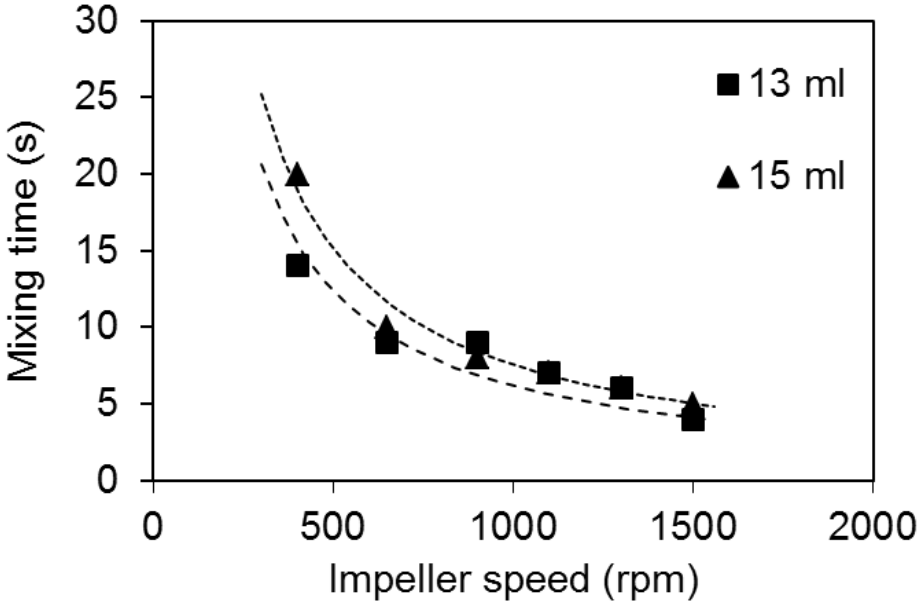
30
25
20
15
10
5
0
Mixing time (s)
0
500
1000
1500
2000
Impeller speed (rpm)
13 ml
15 ml

Figure 7

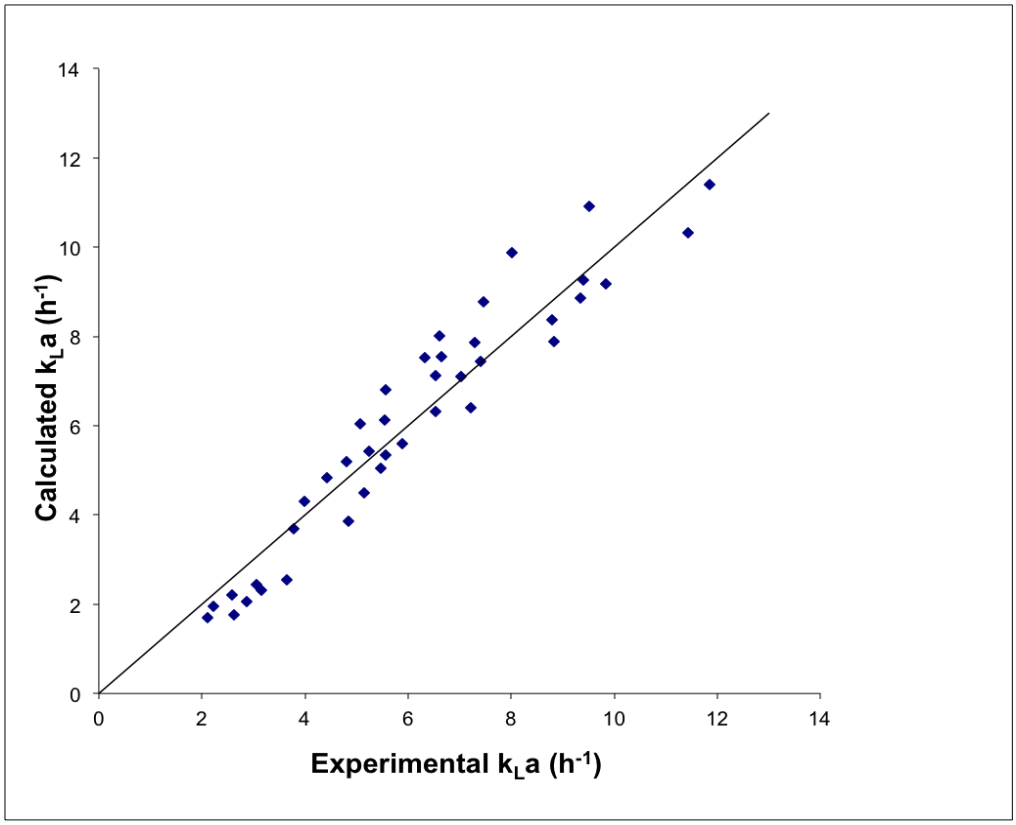

Figure 8

Tables

Impeller Speed (rpm)	Volume (mL)	Measured mixing time (s)
400	13	14
650	13	9
900	13	9
1100	13	7
1300	13	6
1500	13	4
400	15	20
650	15	10
900	15	8
1100	15	7
1300	15	6
1500	15	5

Table 1

Impeller Speed	*P/V*	Volume	Air flow rates, Q_G (mL/min)				
(rpm)	(W/m^3)	(mL)	0	0.11	0.27	0.55	1.0
			Volumetric mass transfer coefficient, k_La (h^{-1})				
300	3.86	13	2.60	3.57	4.17	4.56	5.14
700	48.3	13	4.62	4.92	5.89	6.72	7.54
1000	145	13	6.07	6.26	7.30	8.29	10.28
1200	246	13	6.72	7.20	8.44	9.89	12.69
1500	483	13	7.51	7.49	10.71	13.08	17.58
300	3.35	15	2.05	2.54	2.65	3.76	3.79
700	41.9	15	3.75	4.14	4.67	5.45	5.84
1000	126	15	4.61	5.01	5.83	6.87	7.47
1200	214	15	5.18	5.83	6.95	8.40	8.76
1500	419	15	6.06	6.77	9.80	10.38	12.97

Table 2

Impeller Speed	*P/V*	Volume	Air flow rates, Q_G (mL/min)				
(rpm)	(W/m^3)	(mL)	0	0.11	0.27	0.55	1.0
			Volumetric mass transfer coefficient, k_La (h^{-1})				
300	3.86	13	2.51	2.63	2.86	3.15	3.64
700	48.3	13	4.78	4.84	5.14	5.47	5.89
1000	145	13	6.02	6.12	6.54	7.03	7.60
1200	246	13	7.40	7.22	7.85	8.80	9.40
1500	483	13	9.06	8.83	9.83	11.43	11.85
300	3.35	15	1.98	2.10	2.23	2.58	3.05
700	41.9	15	3.74	3.78	3.99	4.43	5.57
1000	126	15	4.64	4.80	5.08	5.56	732
1200	214	15	5.55	5.55	6.54	6.60	9.35
1500	419	15	6.74	6.64	7.47	8.01	9.51

Table 3

Eq no	A	R^2
1	2.04	0.87
2	1.74	0.91
3	0.017	0.97
4	0.013	0.94

Table 4